Paaua Science Journal

Paper 8

*PaauaSci.J.***2025**, Vol 1 issue 1,101-113

SYNTHESIS, CHARACTERIZATION AND ANTIMICROBIAL STUDIES OF N-(4-METHOXY-2-NITROPHENYL)-2-PHENYLACETAMIDE AND ITS CERIUM (*III*) COMPLEX

Maji, Dorcas Chubiyojo ; Ocheni, Adejoh and Adaji, Muhammed Umar

Prince Abubakar Audu University, Anyigba, Kogi State, Nigeria

majidorcas21@gmail.com (corresponding author)

Received 04-02-2026 **Accepted** 04-03-2026 **Published on line** 04-03-2026

Abstract

The rising occurrence of antimicrobial resistance has intensified the need for novel bioactive compounds with improved therapeutic potential. This paper focused on the synthesis, characterization, and antimicrobial evaluation of the ligand N-(4-methoxy-2-nitrophenyl)-2-phenylacetamide, and its cerium (III) complex. The ligand was synthesized using phenylacetyl chloride as a precursor and subsequently complexed with Cerium (III) Nitrate salts. The characterization of the compound was achieved through UV-Visible spectroscopy, Fourier Transform Infrared Spectroscopy (FTIR), Thermogravimetric Analysis (TGA), solubility studies, which confirmed successful complexation and provided insights into coordination modes. The antimicrobial activities of the ligand and complex were tested against *Staphylococcus aureus*, *Bacillus cereus*, *Escherichia coli*, *Salmonella typhi*, and *Candida albicans* using agar well diffusion and broth microdilution methods. The results revealed that both ligand and complex exhibited significant inhibitory effects, with the Cerium (III) complex generally demonstrating enhanced activity compared to its ligand. Minimum inhibitory concentrations (MIC) ranged between 1.56 and 6.25 mg/ml, and some compounds showed bactericidal and fungicidal effects at relatively low concentrations. The findings highlight the potential of phenylacetyl-derived ligand and its Cerium (III) complex as promising compounds for the development of new antimicrobial agents. This contributes to ongoing efforts in combating drug-resistant infections and offers a foundation for further pharmacological exploration.

Keywords: Antimicrobial, Infections, Ligand and Complex.

Introduction and literature review

Introduction

The challenges of multi-drug resistant microorganisms have reached on alarming level in many countries around the world. Numerous antibiotics have been prescribed and found to be effective on various infectious disorders (Zheng et al., 2024). The reactivity of amides is generally lower compared to other carbonyl compounds like esters and ketones, due to the resonance stabilization provided by the nitrogen atom. However, they can undergo hydrolysis under acidic or basic conditions, forming the corresponding carboxylic acids and amines (Wang et al., 2025).

Literature survey reveals that various drugs e.g. penicillin (antibacterial), pyrazinamide (ant tubercular), indinavir, ritonavir etc. (protease inhibitors as anti-AIDS) contains their particular activities due to the amide linkage present in their structures. Diverse biological properties including Antihistamine, Anti-convoulsant, Anti HIV1 and as potential cocaine abuse therapeutic agent (Xuan et al., 2023). Phenylacetyl chloride is an organic compound with the chemical formula C_8H_7ClO. It is an aromatic acyl chloride, where a phenyl group (C_6H_5) is bonded to an acetyl chloride group (CH_3COCl). This compound was characterized by its use as a reagent in organic synthesis, particularly in the formation of esters and amides (Balachandran et al., 2018). It is commonly utilized in the pharmaceutical industry and in the synthesis of various organic compounds. It serves as a key intermediate in the production of pharmaceuticals, including certain antibiotics and antihistamines.

In addition, it is used in the synthesis of complex molecules in research and development due to its ability to react with nucleophiles and other electrophiles (Kumar et al., 2024). Phenylacetyl chloride a good starting material for synthesizing derivatives of multifunctional ligands of promising bioactive and chelating agents in the study of coordination compounds. It is used as a key precursor in the synthesis of vitamins B which is a powerful inhibitor and building blocks of carbonyl compounds (Mohanasundaram et al., 2021).

The compound is known for its reactivity, particularly in nucleophilic acyl substitution reactions. As with many acyl chlorides, phenylacetyl chloride must be handled with care due to its corrosive nature and potential to release hydrogen chloride gas upon reaction with water or moisture (Le Berre et al., 2020). The choice of Phenyacentyl chloride as a starting material is attributed to its reactivity and potency in molecules design. Complexation of the various derivatives with selected lanthanoid elements are of great interest due to their potent microbial properties (Jalan et al., 2014).

They are several drugs for the treatment of infections arising from wide range of microorganism, and the usage of these drugs over time may have become ineffective as a result of drug resistance. There is need therefore, to develop new compounds which could have curative potency against the resistant organisms. The present work attempts to develop new structural compounds that can be more effective against drug sensitive and resistance to infections. Therefore, the study is to Synthesize, Characterize and carry out antimicrobial study of N-(4-methoxy-2-nitrophenyl)-2-phenylacetamide, and its cerium (III) complex.

Experimental Methods

Experimental

Preparation of N-(4-methoxy-2-nitrophenyl)-2-phenylacetamide

The compound N-(4-methoxy-2-nitrophenyl)-2-phenylacetamide was prepared following literature methods (Atulkumar *et al.,* 2012; Ming-Chihfang, 2013). 0.13mL of 2-phenylacentylchroride was reacted with 0.136 mmole of 4-methyl-2-nitrobenzanamine in 50ml of chloroforam under reflux at 60^0c for 2h. The resultant mixture was filtered to obtain the crystals, which was further stored in a desiccator for further use.

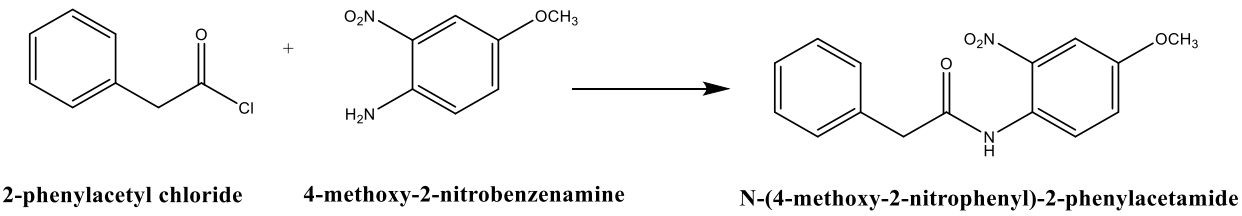

2-phenylacetyl chloride **4-methoxy-2-nitrobenzenamine** **N-(4-methoxy-2-nitrophenyl)-2-phenylacetamide**

Fig.1 Synthesis of N-(4-methoxy-2-nitrophenyl)-2-phenylacetamide

Synthesis of the complex

The cerium (III) complex of the ligand was papered according to the method of (Dalal *et al.,* 2019). The ligand was reacted separately with metal salts using mole ratio 2:1 under the reflux for 2h and the product was filtered to obtain the crystals, which was further stored in a desiccator for further use. The physical properties of the ligand and its complex were studied.

Results and Discussions

Results

Physical properties and solubility properties of the compound and its complex

Table 1 is the physical properties of the synthesized ligand and its complex, while table 2 is the solubility profile in selected solvents.

Table 1: Physical characteristics of synthesized ligand and its complex

Molecular formula	Mol weight	Colour	Texture	% Yield	M.P(^{0}C)
$C_{15}H_{14}N_2O_4$ (L)	286	Orange	Crystals	75	103-107
$C_{15}H_{14}N_2O_4$ (Complex)	4	Orange (burnt)	Crystals	78	110-115

Table 2: Solubility of the Ligand and its Complex

Compounds / Solvents	CH_2Cl_2	MeOH	H_2O	n-hexane	DMF	Acetone	DMSO	CCL_4	C_6H_6	Diethylther
$C_{15}H_{14}N_2O_4$ (Ligand)	S	P.S	IS	P.S	S	S	S	S	S	S
$C_{15}H_{14}N_2O_4$ (Complex)	S	P.S	IS	P.S	S	S	S	S	S	S

Key: S = Insoluble, P.S = Partially Soluble and S = Soluble

Electronic spectra of the ligand and its complex

The UV/Vis absorption spectra of the N-(4-methoxy-2-nitrophenyl)-2-phenylacetamide, and its cerium (III) complex is given in Figs 2. The spectra were obtained as dimethyl sulfuroxide solution at room temperature. The absorption bands are within 200-500 nm.

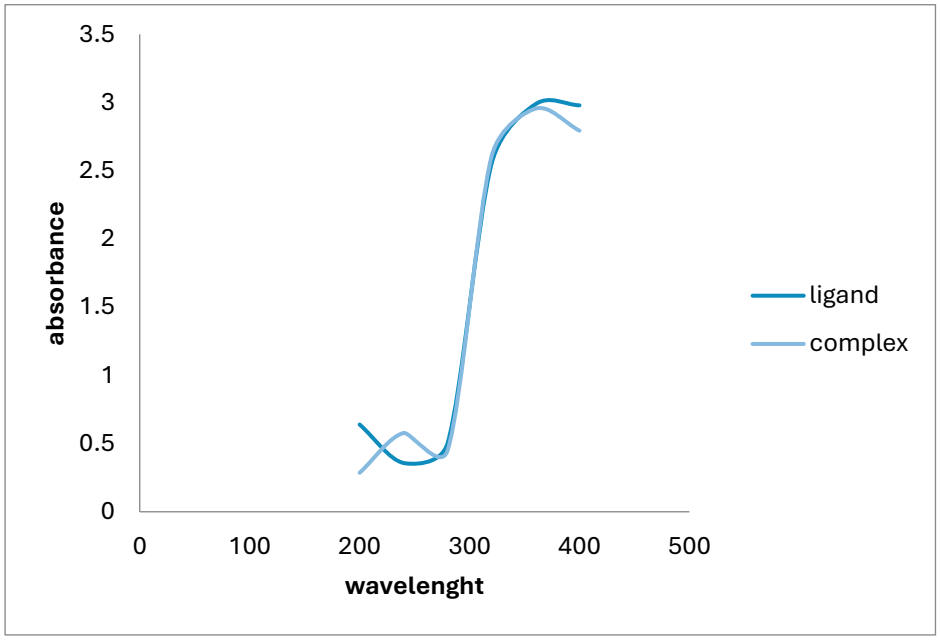

Fig. 2: UV- visible spectra of 4-amino -3-nitrophenyl-2-phenylacetate and its cerium (III) complex

Table 3: Electronic Spectra of the Ligand and its Complexes

Compound	**Absorption nm**	**Absorption cm^{-1}**	**Assignment**	**Geometry**
$C_{15}H_{14}N_2O_4$	400	25000	Low-energy ICT / extended n→π* (ligand-centered)	-
$[Ce(C_{15}H_{14}N_2O_4)_2.3H_2O]$	240 360	41667 27778	240 nm: π→π* (ligand); 360 nm: shifted n→π*/LMCT	distorted square-antiprism

Fourier Transform Infrared Spectra (FTIR) Spectroscopic Analysis

The FTIR spectra of the ligand and its Ce(III) complex provide clear evidence for complexation

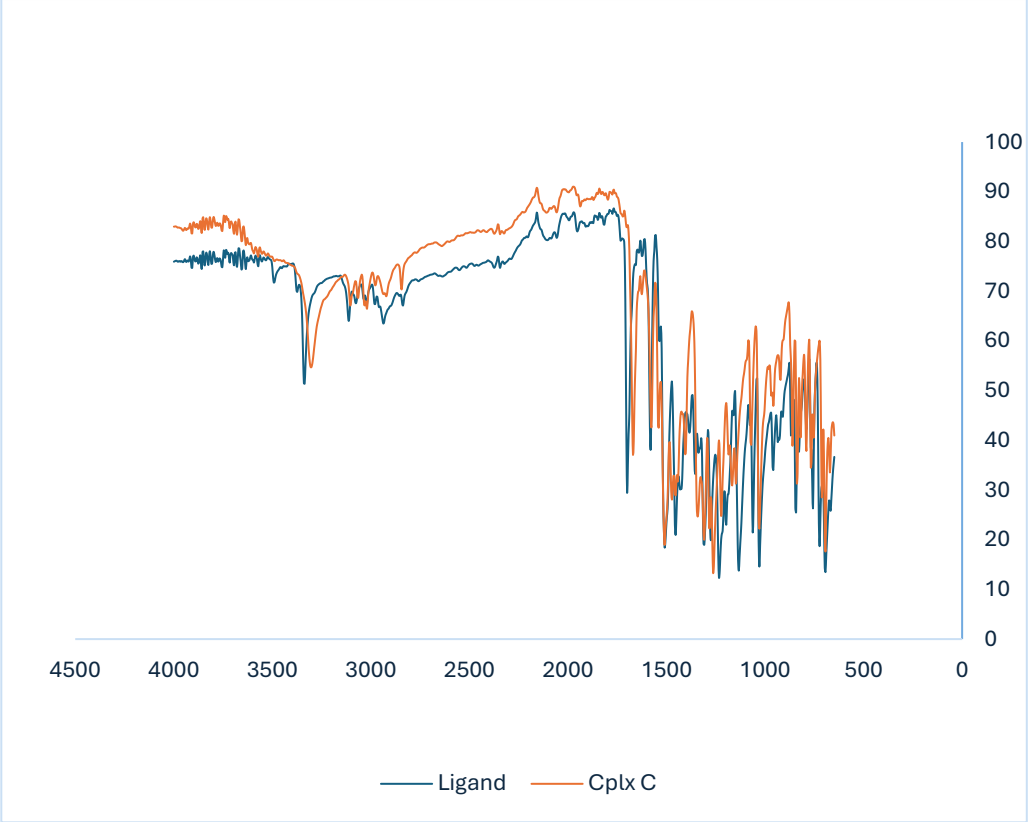

Fig. 3: FTIR spectra of N-(4-methoxy-2-nitrophenyl)-2-phenylacetamide and its complex

Table 4: FTIR Spectra of the ligand and complexes

Molecular formula	**Vibrational frequencies (cm^{-1})**				
	N-O	C=O	N-H	C=C	$-H_2O$
$C_{15}H_{14}N_2O_4$	1580	1700	3339	1509	-
$[Ce(C_{15}H_{14}N_2O_4)_2 \cdot 3H_2O$	1576	1669	3302	1509	3593

Thermogravimetric Curve of the Compound

Thermogravimetric curve of the compound reveal the decomposition properties of the compound as a plot of change in mass of the compound against the temperature and the results are shown in Table 5

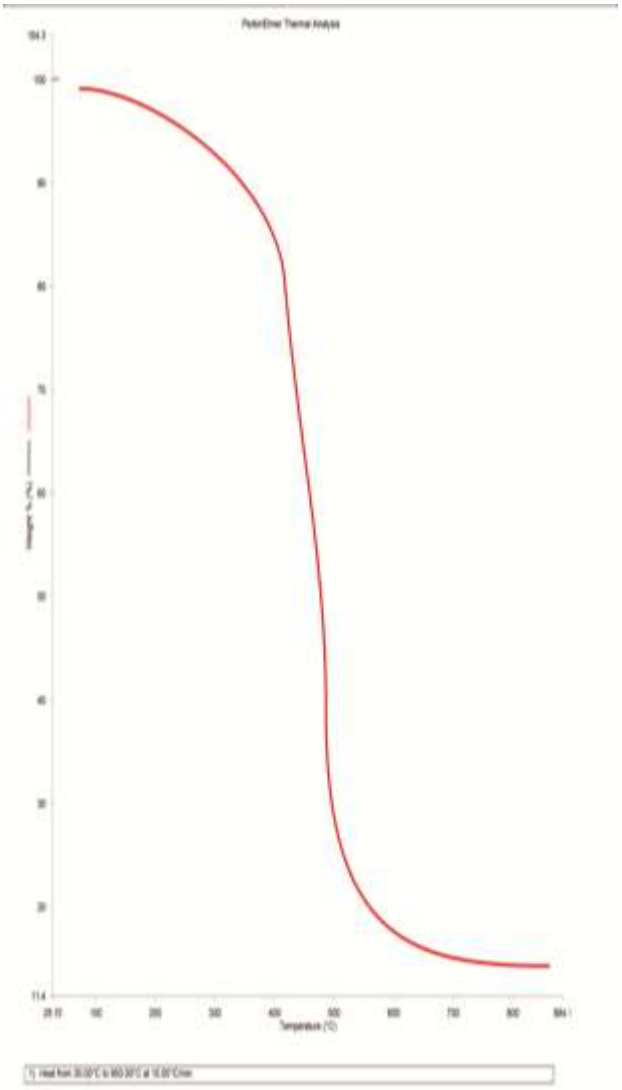

Fig. 4. TGA Curve of $[Ce(C_{15}H_{14}N_2O_4)_2 \cdot 3H_2O]$

Table 5: Thermogravimetric Analysis of Metal complexes

Compounds	Stage	Temp. range (°C)	Mass loss (%) obs.	Mass loss (%) calc.	Assignment
$[Ce(C_{15}H_{14}N_2O_4)_2 \cdot 3H_2O]$		30 – 150	3.5	3.54	Loss of 2 lattice H_2O
		150 – 250	1.9	1.77	Loss of 1 coordinated H_2O
		250 – 600	76.7	77.80	Decomposition of organic ligands (volatile gases) $C_{14}H_{13}N_2O_4$
		>600	17.9	16.89	CeO_2 Residue

Antimicrobial Properties of the Ligand and its Complex

Table 4 shows the antimicrobial properties of the synthesized compound against selected microbes using ketoconazole and erythromycin as control drugs. The compound showed activity against the tested microbes both fungi and bacteria isolates.

Table 6: Antimicrobial activity of the ligand and complexes against selected organisms (zones of inhibition in mm, Mean ± SD, n = 3)

Microorganism	100 mg/mL	50 mg/mL	25 mg/mL	12.5 mg/mL	+ve	-ve
			$C_{15}H_{14}N_2O_4$ ligand			
Bacillus cereus	20.0 ± 0.6	18.0 ± 0.5	16.0 ± 0.6	13.0 ± 0.5	11.0 ± 0.6	0
Staphylococcus aureus	21.0 ± 0.6	19.0 ± 0.5	16.0 ± 0.6	14.0 ± 0.5	10.0 ± 0.6	0
Escherichia coli	19.0 ± 0.6	17.0 ± 0.5	15.0 ± 0.6	13.0 ± 0.5	11.0 ± 0.5	0
Salmonella typhi	20.0 ± 0.6	17.0 ± 0.5	15.0 ± 0.5	11.0 ± 0.5	12.0 ± 0.6	0
Candida albicans	16.0 ± 0.5	14.0 ± 0.5	12.0 ± 0.6	10.0 ± 0.5	10.0 ± 0.5	0
			$[(CeC_{15}H_{14}N_2O_2)_2.3H_2O]$ complex			
Bacillus cereus	22.0 ± 0.6	20.0 ± 0.5	18.0 ± 0.5	16.0 ± 0.5	11.0 ± 0.6	0
Staphylococcus aureus	21.0 ± 0.6	19.0 ± 0.5	17.0 ± 0.6	14.0 ± 0.5	10.0 ± 0.5	0
Escherichia coli	22.0 ± 0.6	20.0 ± 0.5	17.0 ± 0.6	15.0 ± 0.5	11.0 ± 0.5	0
Salmonella typhi	22.0 ± 0.5	19.0 ± 0.6	16.0 ± 0.5	14.0 ± 0.5	12.0 ± 0.6	0
Candida albicans	17.0 ± 0.5	15.0 ± 0.5	13.0 ± 0.5	10.0 ± 0.5	10.0 ± 0.5	0

Table 7: Minimum inhibitory concentration (MIC) and minimum bactericidal (MBC)/fungicidal, MFC) concentrations

Dermatophytes	2-p. acetate complex (mg/ml)		2-p. acetate ligand (mg/ml)	
	MIC	MBC/ MFC	MIC	MBC/ MFC
B. cereus	1.56	6.25	3.125	6.25
Staph. Aureus	3.125	6.25	3.125	12.5
E. coli	3.125	6.25	3.125	12.5
S. typhi	3.125	6.25	6.25	25
C.albicans	3.125	6.25	3.125	6.25

Discussions

The results of physical properties of the synthesized ligand and its complex reveal that the compound is crystal at room temperature, and the compound melted/decomposed at temperatures above 100 ^{0}C. The physicochemical characteristics of the synthesized ligand and the complex shows distinct differences in molecular weight, color, morphology, percentage yield, and melting point. The complex exhibited higher molecular weight than its ligand, consistent with the incorporation of metal centers during coordination. A notable observation was the variation in color: while the ligand was black, its complex maintained a black brown coloration. This difference in physical state highlights the role of crystal packing and intermolecular interactions in determining solid-state properties.

Interestingly, the ligand appeared in two crystal forms with different colors and melting points, suggesting the possibility of polymorphism, a phenomenon where molecules crystallize in more than one lattice arrangement (Onur et al., 2020). The percentage yield for ligand is 75%, while complex is slightly higher at 78%. This modest reduction is typical of coordination syntheses, which often involve additional purification and crystallization steps (Kargar et al., 2024). A significant observation across the dataset is the consistent increase in melting or decomposition temperatures for complex compared with its free ligand. The ligand melted at 103–107 °C, while its complex melted at 110–115 °C. This trend indicates that complex formation enhances thermal stability, likely due to stronger intermolecular interactions and the rigidity imparted by metal ligand coordination. Such stability enhancement upon metal binding has been widely reported for coordination compounds and remains a key property in their functional applications (Chalmardi et al., 2017).

The aromatic amine contains: Methoxy group ($–OCH_3$) which donates electron while the Nitro group ($–NO_2$) is a strong electron-withdrawing compound. The nitro group decreases the nucleophilicity of the amine nitrogen by withdrawing electron density. The methoxy group donates electron density via resonance. The nitro group dominates, so the amine is less nucleophilic than an unsubstituted aniline, meaning: Reaction proceed more slowly and the base is usually required to neutralize HCl (Kargar et al., 2024).

UV–Vis absorptions of organic ligand in the 200–420 nm range usually reflect a combination of intra-ligand $\pi \rightarrow \pi^*$ transitions (high energy, strong bands, typically < 300 nm) and $n \rightarrow \pi^*$ transitions (lower energy, weaker, often 300–400 nm) from lone-pair containing heteroatoms (O, N) conjugated into the π-system (Kasha-type assignments). Upon coordination to a metal center such as cerium, this ligand-centered transitions is commonly perturbed: coordination lowers the energy gap (bathochromic shift) of π or n orbitals and may introduce ligand-to-metal charge transfer (LMCT) bands or metal-centered 4f→5d (or 4f−5d) absorptions for lanthanides. In addition, coordination typically increases molar absorptivity and broadens bands due to increased polarizability and vibronic coupling (Zhou et al., 2019)

Lanthanide ions such as Ce(III) adopt high coordination numbers (commonly 8–10) with flexible geometries (bicapped trigonal prism, square antiprism, distorted dodecahedron), so geometry assignments without structural (X-ray) data remain tentative (Shaji et al., 2004).

The FTIR spectra of the ligand and its corresponding Ce(III) complex provide clear evidence for complexation. For the free ligand, the characteristic stretching vibrations of the C=O is 1700 and N–O group is 1580, while the N-H group is 3339. Upon complexation, these bands underwent significant shifts (e.g., C=O: 1669cm^{-1}; N–H:3302cm^{-1}) confirming that these functional groups are actively involved in coordination with the Ce(III) ion. The N–H stretching vibration, observed between 3339 - 3302cm^{-1} in the free ligand and complex, also exhibited modest downshifts. While such shifts are less pronounced than those expected for direct metal–nitrogen coordination, they point toward secondary interactions. This suggests that the N–H group is not directly coordinated to Ce(III), but rather engaged in hydrogen bonding with coordinated or lattice water molecules within the coordination sphere. This interaction perturbs the vibrational environment of the N–H bond, leading to the observed spectral changes.

The thermal decomposition behaviour of the cerium (IV) complex $[Ce(C_{15}H_{14}N_2O_4)_2 \cdot 3H_2O]$ was investigated using TGA, and the results are summarized in Table 5. The first stage of decomposition occurred within the range of 30–150 °C, showing an observed weight loss of 3.5%, which closely matches the theoretical value of 3.54%. This step corresponds to the removal of two lattice water molecules that are weakly bound and readily lost at relatively low temperatures.

The second stage was observed between 150–250 °C with an experimental mass loss of 1.9% (theoretical 1.77%), which can be attributed to the elimination of one coordinated water molecule. The presence of both lattice and coordinated water is consistent with the proposed formulation of the complex, and the agreement between observed and calculated values supports the stoichiometry. The most significant decomposition occurred between 250–600 °C, where the complex exhibited a large weight loss of 76.7% (theoretical 77.80%). This stage corresponds to the degradation and volatilization of the Schiff base ligands, leading to the breakdown of the organic framework of the complex. The broad temperature range of this stage suggests overlapping decomposition processes involving multiple organic moieties.

Above 600 °C, no substantial weight loss was observed, and a stable residue was obtained. The residue weight corresponded to 17.9%, in good agreement with the theoretical 16.89%, which is assigned to the formation of cerium dioxide (CeO_2). The presence of CeO_2 as the final product is consistent with previous reports on the thermal decomposition of cerium(IV) Schiff base complexes (Ejidike et al., 2025). Overall, the observed decomposition pattern is in close agreement with the calculated theoretical values, confirming the proposed molecular composition and stability of the complex. The results further highlight the thermal robustness of the complex until ligand decomposition occurs, and the eventual formation of CeO_2 underscores the potential application of such complexes as precursors for cerium oxide nanomaterials.

The antimicrobial evaluation of the extract revealed consistent inhibitory activity across all tested organisms. The inhibition zones demonstrated a concentration-dependent trend, with the highest values observed at 100 mg/mL and progressively decreasing at lower concentrations. At 100 mg/mL, *Staphylococcus aureus* displayed the greatest susceptibility (21.0 ± 0.6 mm), significantly surpassing the inhibition recorded for *Candida albicans* (16.0 ± 0.5 mm) at the same concentration ($p < 0.01$). Similarly, *Bacillus cereus* and *Salmonella typhi* both recorded inhibition zones of 20.0 ± 0.6 mm, highlighting the broad-spectrum antibacterial potential of the extract. *Escherichia coli* exhibited slightly lower sensitivity (19.0 ± 0.6 mm), but the inhibition remained comparable to Gram-positive strains. At moderate concentrations (50–25 mg/mL), inhibition zones were still notable, ranging from 19.0 ± 0.5 mm (*S. aureus*) to 12.0 ± 0.6 mm (*C. albicans*). At the lowest concentration tested (12.5 mg/mL), inhibitory activity was reduced but remained measurable across all organisms, indicating that the extract retained residual antimicrobial efficacy even at submaximal doses. When compared with positive controls (erythromycin for bacteria, ketoconazole for fungi)**,** the extract displayed comparable or even superior efficacy at higher concentrations. For example, the inhibition zone of *S. aureus* at 100 mg/mL (21.0 ± 0.6 mm) exceeded that of erythromycin (10.0 ± 0.6 mm), while *C. albicans* inhibition (16.0 ± 0.5 mm) was significantly higher than ketoconazole (10.0 ± 0.5 mm, $p < 0.01$). This suggests that the extract may possess potent bioactive compounds capable of rivaling conventional antibiotics, particularly against Gram-positive bacteria.

The negative control (water) showed no inhibition, confirming that antimicrobial activity was solely due to the extract. The overall findings support that the extract possesses broad-spectrum antimicrobial activity, with greater potency against bacteria compared to fungi. This trend aligns with previous reports that phytochemical-derived metal complexes often display stronger antibacterial properties due to enhanced interactions with bacterial membranes and enzymatic systems (Berhanu et al., 2019). The antimicrobial screening results of the extract demonstrated potent inhibitory effects against all tested organisms, with activity generally increasing in proportion to extract concentration. At 100 mg/mL, maximum inhibition was observed for *Bacillus cereus*, *Escherichia coli*, and *Salmonella typhi* (22.0 ± 0.6 mm each), while *Staphylococcus aureus* and *Candida albicans* exhibited slightly lower inhibition zones (21.0 ± 0.6 mm and 17.0 ± 0.5 mm, respectively). These findings suggest that the extract has strong broad-spectrum antimicrobial activity, particularly against Gram-negative organisms

(*E. coli* and *S. typhi*) which often display higher resistance to conventional antibiotics. At intermediate concentrations (50–25 mg/mL), inhibition zones ranged between 20.0 ± 0.5 mm (*E. coli*, *B. cereus*) and 13.0 ± 0.5 mm (*C. albicans*). At the lowest concentration tested (12.5 mg/mL), the extract still retained inhibitory potential, though reduced, with inhibition zones of 10.0 ± 0.5 mm (*C. albicans*) to 16.0 ± 0.5 mm (*B. cereus*). This demonstrates a clear dose–response relationship, consistent with concentration-dependent activity of phytochemical-rich extracts.

Comparisons with positive controls revealed that the extract at higher concentrations (≥50 mg/mL) generally outperformed standard antibiotics. For example, the inhibition of *E. coli* at 100 mg/mL (22.0 ± 0.6 mm) was double that of erythromycin (11.0 ± 0.5 mm), while *C. albicans* inhibition (17.0 ± 0.5 mm) surpassed ketoconazole (10.0 ± 0.5 mm). Such potency underscores the potential of the extract as an alternative antimicrobial agent, particularly where multidrug resistance is a concern. The absence of inhibition in the negative control (water) validates that the antimicrobial activity arises solely from the extract. The higher sensitivity of bacteria compared to fungi suggests that the extract's bioactive components may preferentially target bacterial cell walls and membranes, consistent with previously reported mechanisms of plant-derived metal complexes and Schiff base derivatives (Fernández et al., 2007). The antimicrobial activity results of the extract are summarized in table 6. The data reveal a clear dose-dependent inhibition of microbial growth, with higher concentrations producing broader inhibition zones across all tested microorganisms.

Overall, these findings confirm the extract's broad-spectrum antimicrobial activity, particularly strong against bacterial strains, with highest sensitivity observed for *B. cereus* and *S. typhi*. The comparatively weaker antifungal activity suggests possible differences in the mode of action of bioactive components against fungal cell walls compared to bacterial membranes. These results align with previous reports that phytochemical-rich extracts often exhibit stronger antibacterial than antifungal properties (Palanimurugan & Kulandaisamy, 2018).

Conclusions

This research successfully synthesized, characterized, and evaluated the antimicrobial activities of N-(4-methoxy-2-nitrophenyl)-2-phenylacetamide and its cerium (III) complex. The work was motivated by the urgent need to develop new chemical entities with therapeutic potential in response to rising antimicrobial resistance. By combining synthetic organic chemistry with coordination chemistry, the study demonstrated that metal complexation significantly modifies the physicochemical and biological behavior of ligands, enhancing their performance as antimicrobial agents. From the spectroscopic characterizations (UV-Vis, FTIR, TGA, and NMR), evidence of successful ligand synthesis and metal coordination was obtained. Shifts in functional group vibrations, modifications in thermal decomposition patterns, and changes in proton environments all confirmed the expected structural transformations. These results align with literature reports that metal-ligand interactions induce new bonding environments, stabilizing the complexes and improving their functional properties (Ocheni *et al.,* 2012; Ming-Chihfang, 2013; Douglass *et al.,* 2014; Lisa, 2019; Dalal *et al.,* 2019). Importantly, the complexes retained the core structural integrity of the ligands while exhibiting new properties that conferred enhanced stability and reactivity. Biological evaluations against selected microorganisms—including *Staphylococcus aureus, Bacillus cereus, Escherichia coli, Salmonella typhi*, and *Candida albicans* revealed that both ligands and their complexes

exhibited inhibitory effects, though the complexes generally displayed stronger and broader antimicrobial activity. The observed inhibition zones and minimum inhibitory concentrations (MIC) confirmed the role of cerium(III) coordination in potentiating antimicrobial efficacy. These findings validate earlier reports that lanthanide-based complexes possess superior antimicrobial properties due to their ability to interfere with microbial metabolic pathways, alter cell wall permeability, and disrupt enzymatic functions. The research also highlighted differential sensitivity of microbes to the synthesized compounds. Gram-positive bacteria, notably *Staphylococcus aureus* and *Bacillus cereus*, were generally more susceptible compared to Gram-negative *Escherichia coli* and *Salmonella typhi*, while *Candida albicans* exhibited moderate susceptibility. These variations are consistent with the structural differences in microbial cell walls and their defense mechanisms. Nonetheless, the broad activity spectrum of the synthesized compounds positions them as promising leads for the development of new antimicrobial agents. The implications of this work are significant. First, it demonstrates that simple modifications of phenylacetyl-based ligands can yield compounds with improved antimicrobial performance. Second, it confirms that coordination with lanthanide metals, particularly cerium(III), enhances biological activity and stability of organic molecules. Third, the study contributes valuable knowledge to the growing body of work on metal-based pharmaceuticals, suggesting that such compounds could serve as alternatives or complements to existing drugs, especially in the fight against resistant pathogens. However, the study also underscores certain limitations. While in vitro antimicrobial tests provided valuable insights, further in vivo studies are required to confirm safety, bioavailability, and therapeutic efficacy. In addition, structural optimization through computational modeling and crystallographic studies could provide deeper understanding of binding mechanisms and structure-activity relationships. Expanding the scope of tested microbes, including multi-drug resistant clinical isolates, would also strengthen the practical relevance of the findings. The study provides a foundation for future research into lanthanide-based drug design and highlights the potential of synthetic chemistry in addressing the global challenge of antimicrobial resistance. Continued efforts in this direction may lead to the development of novel, more effective, and safer therapeutic agents that can supplement or replace conventional antibiotics.

References

Atulkumar, T., Subshil, G., Shilpa, K., Abhaykumar, M., Shashi, A. (2012). Synthesis and pharmacological evealuation of 1-benz-hydydryl piperazine derivatives. *International Journal of Phavmaceutical Sciences and Research.* 3(1), 312-217.

Balachandran, C., Haribabu, J., Jeyalakshmi, K., Bhuvanesh, N. S. P., Karvembu, R., Emi, N., & Awale, S. (2018). Nickel(II) bis(isatin thiosemicarbazone) complexes induced apoptosis through mitochondrial signaling pathway and G0/G1 cell cycle arrest in IM-9 cells. *Journal of Inorganic Biochemistry*, *182*, 208–221. https://doi.org/10.1016/j.jinorgbio.2018.02.014

Berhanu, A. L., Gaurav, Mohiuddin, I., Malik, A. K., Aulakh, J. S., Kumar, V., & Kim, K. H. (2019). A review of the applications of Schiff bases as optical chemical sensors. *TrAC - Trends in Analytical Chemistry*, *116*, 74–91. https://doi.org/10.1016/j.trac.2019.04.025

Chalmardi, G. B., Tajbakhsh, M., Bekhradnia, A., & Hosseinzadeh, R. (2017). A highly sensitive and selective novel fluorescent chemosensor for detection of Cr3+ based on a Schiff base. *Inorganica Chimica Acta*, *462*, 241–248. https://doi.org/10.1016/j.ica.2017.03.041

Dalal, M. I., Hana, S. M., Hana, H. L. (2019). Synthesis and Characterization New Schiff Base Derivatives and Their Complexes with Zn (II) and Ni (II). *Journal of Applied Chemistry (IOSR-JAC) e-ISSN:* 12(8), 24-34.

Douglas, A. L. Otte, D. E. Borchmann, C. L., Marcus W. (2014). CNMR Spectroscopy for the Quantitative Determination of Compound Ratios and Polymer End Groups, *National Center for Biotechnology Information,* 16(6), 1566-1569.

Ejidike, I. P., Direm, A., Parlak, C., Olaleru, S. A., Adetunji, C. O., Mtunzi, F. M., Ata, A., Eze, M. O., Clayton, H. S., Ajibade, P. A., & Hollett, J. W. (2025). DNA gyrase inhibition by Ni(II)-Schiff base complexes via in silico molecular docking studies: Spectroscopic, DFT calculations and in vitro pharmacological assessment. *Results in Chemistry*, *15*(March), 102219. https://doi.org/10.1016/j.rechem.2025.102219

Fernández, J., Navasa, M., Planas, R., Montoliu, S., Monfort, D., Soriano, G., Vila, C., Pardo, A., Quintero, E., Vargas, V., Such, J., Ginès, P., & Arroyo, V. (2007). Primary Prophylaxis of Spontaneous Bacterial Peritonitis Delays Hepatorenal Syndrome and Improves Survival in Cirrhosis. *Gastroenterology*, *133*(3), 818–824. https://doi.org/10.1053/j.gastro.2007.06.065

Jalan, R., Fernandez, J., Wiest, R., Schnabl, B., Moreau, R., Angeli, P., Stadlbauer, V., Gustot, T., Bernardi, M., Canton, R., Albillos, A., Lammert, F., Wilmer, A., Mookerjee, R., Vila, J., Garcia-Martinez, R., Wendon, J., Such, J., Cordoba, J., … Ginès, P. (2014). Bacterial infections in cirrhosis: A position statement based on the EASL Special Conference 2013. *Journal of Hepatology*, *60*(6), 1310–1324. https://doi.org/10.1016/j.jhep.2014.01.024

Kargar, H., Fallah-Mehrjardi, M., & Munawar, K. S. (2024). Metal complexes incorporating tridentate ONO pyridyl hydrazone Schiff base ligands: Crystal structure, characterization and applications. *Coordination Chemistry Reviews*, *501*. https://doi.org/10.1016/j.ccr.2023.215587

Kumar, M., Singh, A. K., Singh, V. K., Yadav, R. K., Singh, A. P., & Singh, S. (2024). Recent developments in the biological activities of 3d-metal complexes with salicylaldehyde-based N, O-donor Schiff base ligands. *Coordination Chemistry Reviews*, *505*. https://doi.org/10.1016/j.ccr.2024.215663

Le Berre, C., Sandborn, W. J., Aridhi, S., Devignes, M. D., Fournier, L., Smaïl-Tabbone, M., Danese, S., & Peyrin-Biroulet, L. (2020). Application of Artificial Intelligence to Gastroenterology and Hepatology. *Gastroenterology*, *158*(1), 76-94.e2. https://doi.org/10.1053/j.gastro.2019.08.058

Lisa, N. (2019). Step by step procedure for melting point. Organic laboratory techniques licensed under a creative common international license.

Ming-Chihfang, F., (2013). *Synthesis and Stabilization of Selected Heterocyclic Aroma Compounds.* Dissertation submitted in partial fulfillment of the requirements for the degree of doctor of philosophy in food Sciences Nutrition the University of Illinois Urbanan Champaign USA.

Mohanasundaram, D., Bhaskar, R., Gangatharan Vinoth Kumar, G., Rajesh, J., & Rajagopal, G. (2021). A quinoline based Schiff base as a turn-on fluorescence chemosensor for selective and robust detection of Cd2+ ion in semi-aqueous medium. *Microchemical Journal*, *164*. https://doi.org/10.1016/j.microc.2021.106030

Ocheni, A., ,Ukoha, P. O., Onoja, P. K. (2016). Synthesis, Characterization and Preliminary Microbial Studies of 4-{[(E)–1h–Indol– 3h–Lmethylidene]Amino}–1,5-Dimethyl-2-Phenyl-1,2-Dihydro-3h-Pyrazol–3-One and Its Al(Iii), In(Iii) and Tl(I) Complexes, ***Advances in Natural Science*****,** 9(2), 1-6.

Onur, S., Güngör, S. A., Tümer, F., & Tümer, M. (2020). The color, photophysical and electrochemical properties of azo-imine ligands and their copper(II) and platinium(II) complexes. *Journal of Molecular Structure*, *1200*, 127135. https://doi.org/10.1016/J.MOLSTRUC.2019.127135

Shaji, S., Eappen, S. M., Rasheed, T. M. A., & Nair, K. P. R. (2004). NIR vibrational overtone spectra of N-methylaniline, N,N-dimethylaniline and N,N-diethylaniline - A conformational structural analysis using local mode model. *Spectrochimica Acta - Part A: Molecular and Biomolecular Spectroscopy*, *60*(1–2), 351–355. https://doi.org/10.1016/S1386-1425(03)00233-6

Wang, K., Li, S., Jing, X., Shang, W., Yan, T., Bai, X., Zhao, R., & Ma, Y. (2025). Highly sensitive fluorescence detection of chlortetracycline and tetracycline residues in food samples based on a Zn(II) coordination polymer. *Spectrochimica Acta - Part A: Molecular and Biomolecular Spectroscopy*, *343*. https://doi.org/10.1016/j.saa.2025.126587

Xuan, J., Feng, W., Wang, J., Wang, R., Zhang, B., Bo, L., Chen, Z. S., Yang, H., & Sun, L. (2023). Antimicrobial peptides for combating drug-resistant bacterial infections. *Drug Resistance Updates*, *68*. https://doi.org/10.1016/j.drup.2023.100954

Zheng, D., Fang, Z., & Sun, J. (2024). Which Is More Clinically Relevant: End-of-Treatment or Off-Treatment Predictors of Hepatitis B Relapse and Surface Antigen Loss? *Gastroenterology*, *166*(6), 1193–1194. https://doi.org/10.1053/j.gastro.2023.10.020

Zhou, J., Ran, Z. F., Liu, Q., Xu, Z. X., Xiong, Y. H., Fang, L., & Guo, L. P. (2019). Jasmonic acid serves as a signal role in smoke-isolated butenolide-induced tanshinones biosynthesis in Salvia miltiorrhiza hairy root. *South African Journal of Botany*, *121*, 355–359. https://doi.org/10.1016/j.sajb.2018.10.029

By checking the following box, the senior author acknowledges that they and the other authors have read, understood, and complied with the Instructions to Authors (ItA).

☐